Integrated, Eddy-Current-Based Sensing of Rotor Position for Magnetic Levitation

Patricio Peralta, Sean Thomas and Yves Perriard
Laboratory of Integrated Actuators
École polytechnique fédérale de Lausanne
Neuchâtel, Switzerland
{juan.peraltafierro, sean.thomas, yves.perriard}@epfl.ch

***Abstract*—Magnetically-levitated drives are compelling in applications where long-lifetime operation or process chamber encapsulation is a requirement. To exploit these advantages, contactless position sensors are needed for position information of the rotor. Off-the-market sensor technologies render high-performance magnetic levitation possible; yet their system integration may be challenging.**

In this work, a position sensing system based on Eddy-current generation is proposed. A single integrated circuit excites an array of four opposing miniature coils, allowing for differential measurement. Coupled to a micro-controller, it can estimate position of an electrically-conductive target —in this case the rotor of a magnetically-levitated drive— at high sampling rates.

***Index Terms*—Sensor, Motion Control, Magnetic Bearings**

I. Introduction

Magnetic levitation enables the contactless operation of electric drives, thus broadening the scope of their applications. Nevertheless, magnetic levitation can deliver its full potential and be economically competitive only when the complete drive system is seamlessly integrated [1]. In this domain, sensor technologies are fundamental, because they permit the estimation of the position of the magnetically-levitated rotor in a chamber or its airgap.

Reviews [2], [3] refer to optical, capacitive, inductive and Eddy-current-based approaches as suitable for contactless-position measurement for magnetic levitation. This work reviews the implementation of an Eddy-current-based approach, given their robustness to electromagnetic noise and dust and their high-bandwidth operation.

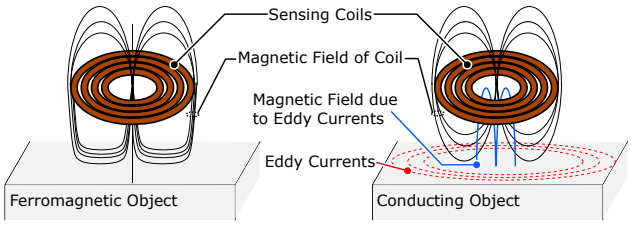

Fig. 1. Contactless position measurement techniques that use sensing coils, exploiting inductance changes due to ferromagnetic targets (left) and the eddy-current effect due to conductive targets (right).

The proposed system has a relatively low footprint and can be used to excite particularly small coils. This enables its integration in narrow spaces and therefore does not require special constructive measures for its mounting.

The inductive and eddy current principles are depicted in Fig. 1. For the inductive principle, a coil (which may or may not have a ferromagnetic core) is excited by an alternating voltage, thus generating a magnetic flux. If a ferromagnetic object approaches the coil, magnetic flux through the coil increases, and appears as an increase in coil inductance. This principle is naturally not suited for non-ferromagnetic targets such as rare-earth permanent magnet (PM) rotors.

Analogously, the coil can be excited by a high-frequency voltage. If an electrically conductive target (such as a PM and its coating), approaches the coil, Eddy-currents are induced inside it. These currents subsequently create a magnetic flux against the coil, thus decreasing the total flux and its inductance. The exploitation of this principle has already rendered high-speed rotation with magnetic bearings possible [4].

Eddy-current-based position systems can be implemented differently. On one hand, off-the-market, ready solutions are available [5], [6]. Although these are tunable and flexible, they are bulky and expensive, hence curtailing its potential for system integration. More compact, solutions can be implemented, but are highly system-specific. Among these, both analog [7]–[9] and digital [10], [11] demodulation techniques have been implemented.

In this work, a low-cost, differential position sensing sys-

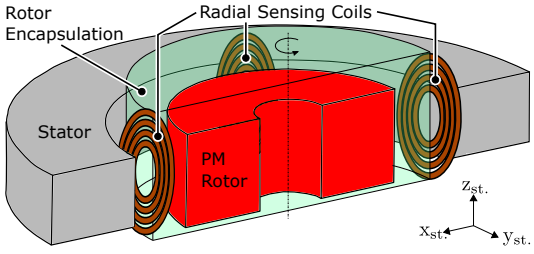

Fig. 2. Sensing coils are placed inside the airgap of a magnetically-levitated motor to measure the radial position (in x and y direction) of its electrically-conductive rotor. Without loss of generality, the sensing system is tested on the here-shown permanent-magnet disc-drive.

978-1-7281-5826-6/20/$31.00 ©2020 IEEE

tem that employs off-the-market components is presented. It communicates via I^{2}C protocol, and can be tuned to use a vast array of coils. Once the sensor array is presented, different positions and excitation frequencies for the sensing coils are tested and rated according to their sensitivity to target movement. Strategies to shield the sensing coils from unwanted noise, and its robustness against it are presented.

II. Hardware

A. Microcontroller and Integrated Circuit

To excite and calculate the inductance of the sensing coils, an off-the-market *Texas Instruments* Inductance to Digital Converter LDC1314 Integrated Circuit (IC) [12] is employed.

The LDC1314 IC can independently manage up to four different coils and communicate with a micro-controller via I^{2}C. This configuration suffices for differential measurement in the $x-y$ axes, and could be managed with position sample rates of 1.9 kHz for the 4 channels. This way, an LDC plus a Delfino Launchpad serve as a *integral* position measurement system.

The LDC1314 IC is soldered onto a PCB, which also offers the filtering capabilities of Fig. 6 for the sensing coil. The fabricated PCB is pin compatible with the Launchpad [13] micro-controller series, that communicates with the LDC and calculates the differential measurement.

The IC excites the parallel LCR resonant tank of Fig. 6, and finds its resonating frequency f_{res}. This is approximately

$$f_{\text{res}}(x) = \frac{1}{2\pi} \frac{1}{\sqrt{L_{\text{coil}}(x) \cdot C_{\text{tank}}}}, \tag{1}$$

with $L(x)_{\text{coil}}$ and C_{tank} the apparent inductance of the sensing coil as a function of its distance x to the target and the installed resonant capacitor, respectively.

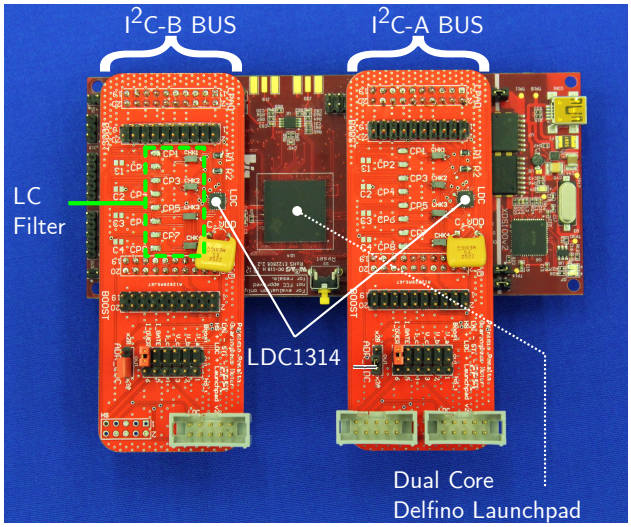

Fig. 3. Delfino Launchpad with two LDC1314 modules. The latter are mounted on separate I^{2}C buses and controlled by separate CPUs of the microcontroller. This enables doubling the position sensing sampling rate that would have been possible using one CPU and one I^{2}C bus. The differential measurement of each axis is output on a DAC.

Although originally meant to measure inductance, the excitation frequency of the coil can be set with C_{tank}. Low C_{tank} values permit the exploitation of the IC and its sensing coil as an Eddy-current position sensor system. The value of $L_{\text{coil}}(x)$ changes in the proximity of a conductive object, as portrayed in Fig. 1, so the frequency f_{res} is thus a function of target distance x is ultimately mapped onto a 12-bit value.

Optionally, and aiming towards faster sampling rates, each differential pair of x and y signals are handled separately, on separate buses and separate cores of the Delfino Launchpad. The differential signals of the axes are each sampled as shown in Fig. 15 and output at the same sampling rate of 3.89 kHz at two of the 12-bit Digital to Analog Converter (DAC) of the microcontroller. This way, two LDC ICs plus a Delfino Launchpad serve as a *integral* position measurement system.

B. Sensing Coils

Three sensing coil, shown in Fig. 4, are tested for position measurement purposes. They are comparable in dimensions, so that their measuring range is also comparable [12].

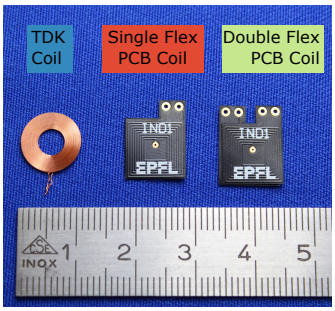

Fig. 4. Sensing coils for Eddy-current position sensing.

The 400 μm thin TDK coil [14] is intended for wireless energy transfer purposes. Its sensing performance is compared to that of a 150 μm thin, 2-layer Flex PCB square coil, designed in [15]. This coil is shown and tested in single and series (double) configuration, to analyze the effect of the increased inductance upon sensing properties.

Fig. 5 shows that the TDK coils and double Flex PCB Coil have comparable inductance, with the double Flex PCB Coil being clearly less resistive. This makes them preferable from the sensing point of view [12]. Moreover, they are thinner, so they can be more easily integrated into a bearingless drive.

C. Shielding and Filtering

The sensing coils are installed in the magnetic airgap as in Fig. 2. At this location, they are prone to disturbances coming from the excitation of the motor. The disturbances can become critical if high dv/dt signals such as Pulsed Width Modulation (PWM) strategies for motor current control are implemented.

At the same time, it is desirable that the sensing coils only measure the change of inductance due to the rotor position, and not of eventual vibrations of other conductive components inside the airgap, i.e. towards the stator of Fig. 2.

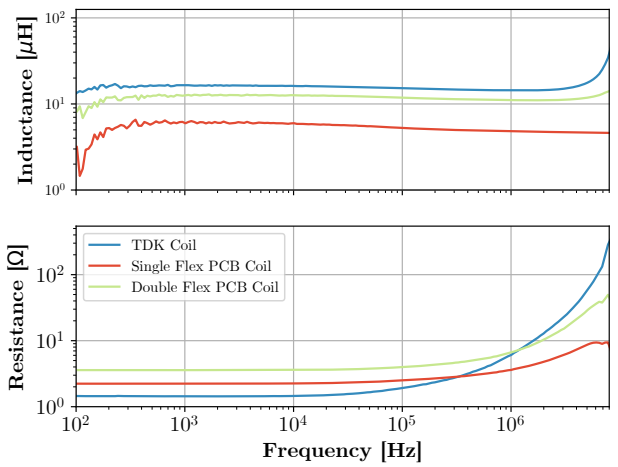

Fig. 5. Measured series inductance and resistance characteristics of the tested sensing coils of Fig. 4.

To address the first issue, an LC filter composed of a choke inductance and a shunt capacitor is implemented. It is placed before the resonant between the LDC terminals and the LCR resonant tank [16], as seen in Fig. 6. This passive filter helps suppress common-node electromagnetic radiation in the airgap, which might be picked up by the sensing coils.

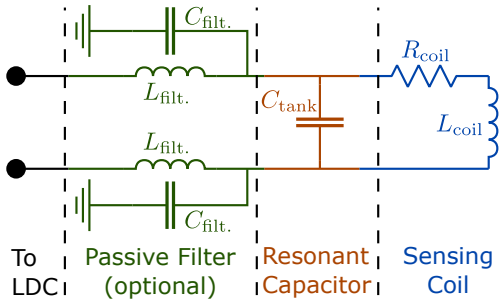

Fig. 6. A resonant capacitor C_{tank} is connected in parallel to the sensing coil. Its terminals are connected to a passive LC filter. The filter aids noise suppression and stable LCR tank resonance.

For the second issue, the Flex PCB from Fig. 7 is conceived [17]. The open and orthogonal paths decrease the sensor sensitivity towards undesired targets and are connected to ground. The PCB is then rolled-around the sensing coils.

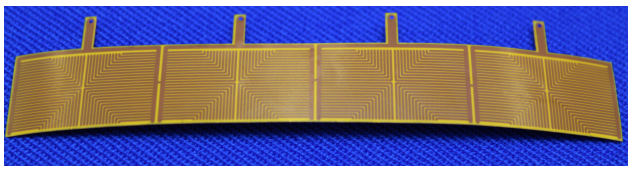

Fig. 7. Flex PCB for sensor shielding purposes. The four shielding units cover the $x - y$ differential sensors.

D. Flexibility and Cost of Proposed System

The proposed sensor system can be connected to sensing coils of different types and is thus not limited to standardized probes. This also enables shortening or enlarging the range of the target distance to be measured [12], as long as the LDC can provide enough excitation current and the C_{tank} coupled to the coil results in a f_{res} that lays inside the capabilities of the LDC. This renders the approach very flexible.

The minimal configuration of this system and the here-presented configuration with the Launchpad microcontroller platform are rather inexpensive, as described in Table I. Passive components, pin devices and PCB integration are excluded from this calculation.

Considering the prices of Table I, it is observed that the coils make up a considerable parts of the costs of the proposed system.

III. Test Bench and Sensor Characterization

A. Test Bench

Figure 8 displays the setup employed to characterize the various sensing coils. Mounted on the XYZ linear stage, a slotless stator made out of Metglas [18] is displaced relative to a fixed, annular NdFeB [19] rotor. The sensor characteristic for a mechanical clearance of up to 2250 μm is analyzed, despite the intended configuration being conceived to levitate inside a 1000 μm clearance.

Sensing coils X^+ and X^- are placed radially in the magnetic airgap, as indicated in Fig. 2 and Fig. 8. Since various sensing coils and capacitor values are implemented, the LDC1314 Evaluation Module along its GUI are employed for sensor characterization. The GUI allows for a swift configuration of the LDC to its sensing coils. The LDC sensor data is logged at 20 Hz and is ultimately paired with the position information measured by a laser displacement sensor.

TABLE I
Approximate Costs for the Eddy-Current-Based Position System. Prices Obtained from *TI* and *PCBgogo* for Low Quantities.

Component	Total Cost [USD]
Minimal Configuration	
1 x TMS320F28379D Microcontroller	13
2 x LDC1314RGHR	2.6
Total	15.6
Presented Configuration	
1 x LAUNCHXL-F28379D	33.8
2 x LDC1314RGHR	2.6
1 x Flex PCB Shielding	10.6
Total	47
Sensing Coil Set Possibilities	
4 x TDK coils	23.3
4 x Single Flex PCB coils	10.4
4 x Double Flex PCB coils	20.8

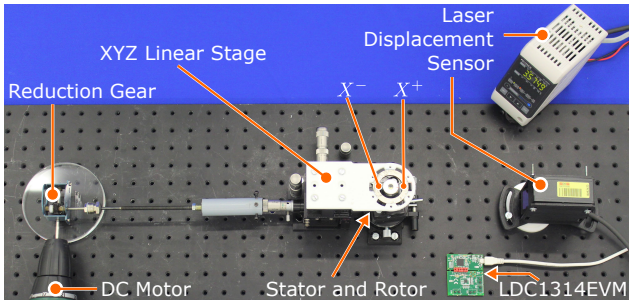

Fig. 8. Test bench setup. A linear stage displaces the stator relative to the rotor. Its x axis is driven at fixed speed thanks to a DC motor and a reduction gear. The test-bench position is corroborated with a laser displacement sensor, and the result of digital inductance conversion of the coils is recorded by the GUI of the LDC1314 EVM.

B. Sensor Characterization

Sensor response is characterized on the x (radial) and also z (axial) direction. Initially, sensor system is characterized by its accuracy when measuring the radial displacement on the airgap. Additionally, the dependence of this radial sensitivity upon axial target displacement is also studied.

It is desirable that axial rotor z position does not affect the sensitivity of the sensor system in x direction. This could modify sensor gain inside the levitation control loops, eventually destabilizing operation.

Table II describes the measured sensor configurations. Capacitor values can be converted to the central resonating frequencies f^*_{res} of Fig. 11 by using Eq. (1) with $L_{\text{coil}}(x = 0 \text{ mm})$. Figure 9 is an example of one measurement set, at a given z rotor position.

TABLE II
MEASURED CONFIGURATIONS. FOR EACH COIL TYPE AND C_{tank}, RADIAL DISPLACEMENTS BETWEEN $x = -2250 : 2250$ μM ARE TESTED, EACH FOR AXIAL DISPLACEMENTS $z = 0 : 500 : 3500$ μM.

Coil Type	C_{tank} [pF]
TDK Coil	1, 3.9, 27, 100
Single Flex PCB Coil	2.2, 8.2, 56, 220
Double Flex PCB Coil	1.2, 3.9, 30, 115

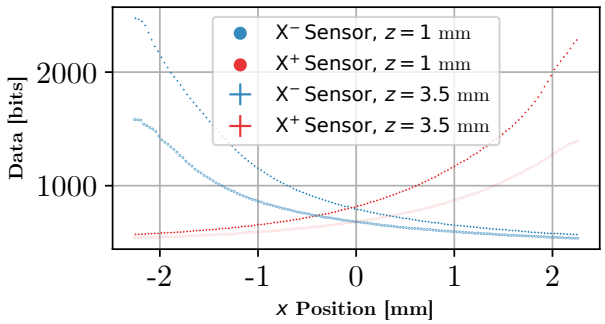

Fig. 9. Logged sensor data of Double Flex PCB Coil with C_{tank} = 30 pF at two different z heights. Each single sensor displays a non-linear characteristic with position; yet their difference delivers a more linear picture, see Fig. 10. Displacing the rotor axially decreases the signal amplitude across the x axis.

IV. Experimental Results

A. Position Curves and Fitting

The differential pair of sensing coils are placed within the stator and their corresponding data is recorded as their relative position to the rotor is changed. These data points are plotted against the position values recorded by the laser displacement sensor as shown in Fig. 10. The data coming from a single sensor is clearly non-linear thus the need of a differential sensor array.

Along the whole x axis measurement, it can be appreciated that the *differential* data follows a cubic function. A third order polynomial can be initially fit to the differential data with good results if a wide distance range is to be characterized.

As a consequence, a simple linear regression throughout the whole x range fits the data poorly due to its non-linear nature. It is thus more meaningful to characterize the sensor around $x = 0$ mm, i.e. for a rotor levitated at the center of the airgap. To quantify the linearity around this interest point, a weighted least square regression is performed where the weights are a Gaussian distribution with σ = 1.2 mm around μ = 0 mm. This way, 95% of the weight for the regression is put around $x = [-1.2, 1.2]$ mm.

B. Sensor Resolution of Tested Configuration

The sensor configurations proposed in Table II are rated in terms of resolution. Resolution represents the minimum displacement that can be detected using the 12-bit output of the LDC134 integrated circuit. It is thus defined as the inverse of the slope of the linear regression line calculated around the centre of the differential sensor data of Fig. 10.

Figure 11 shows the sensitivity of the different inductances excited at central resonant frequency f^*_{res} due to their coupled

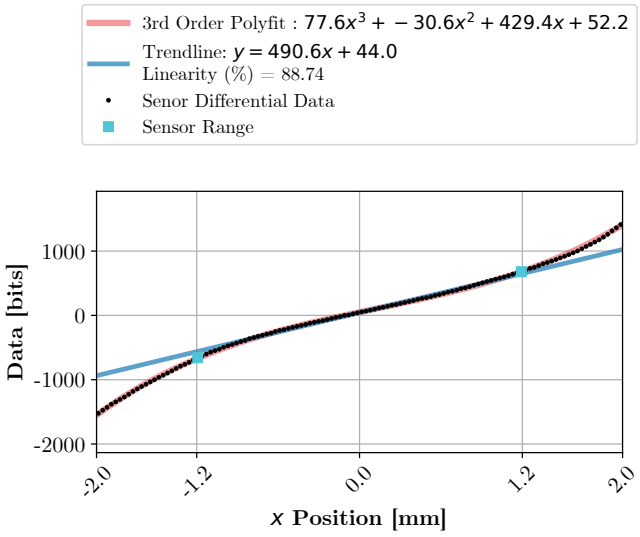

Fig. 10. Differential measurement $X_{\text{POS}} = X^- - X^+$ of rotor position on the x axis. The complete sensor characteristic is best fit by a third degree polynomial, yet it can be linearized around $x = 0$ mm with high accuracy.

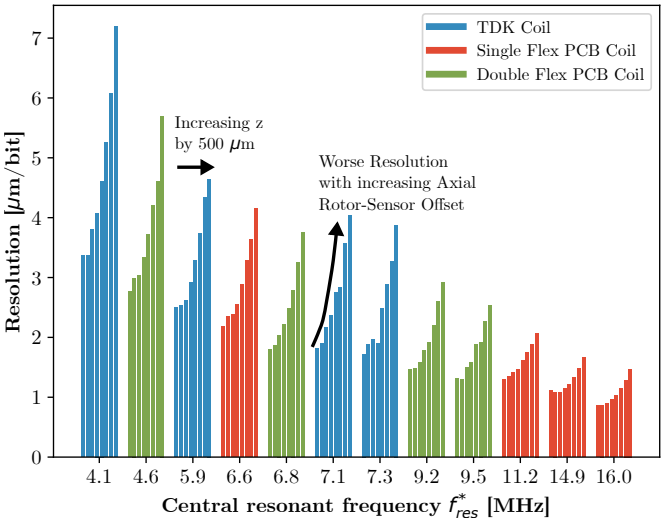

Fig. 11. Resolution of the tested configurations, spawned from Table II. Higher frequencies allow for higher sensitivities. Axially displacing the rotor away from the sensors has a significant impact upon sensor resolution.

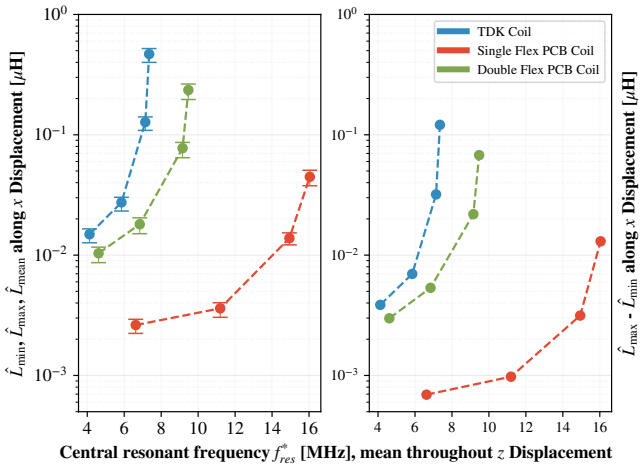

Fig. 12. The dependence of frequency spread $\Delta\hat{L}$ upon central resonant frequency f^*_{res}. Higher f^*_{res} values lead to higher changes of measured inductance in the sensing coils, which translates to better resolutions. Given a certain coil, this should be excited at high-frequencies.

capacitors. The different bars show the sensitivity at different z axial displacements.

It can be seen that the higher the resonant frequency f^*_{res}, the better the resolution, i.e. a smaller rotor displacement can be detected by the sensor system. In this context, the Single Flex PCB Coils result in the best resolution, as their small inductance favour high resonant frequencies.

Analyzing each coil type separately, increasing the frequency improves the measurement resolution. On the other hand, if the rotor is axially displaced, the resolution deteriorates drastically.

C. Frequency-dependence of Sensor Resolution

Bit values of the LDC1314 can be converted to actual inductance values [12]. For each sensor configuration, the maximum, minimum and mean estimated inductance of the sensing coils, $\hat{L}_{\text{max}}$, $\hat{L}_{\text{min}}$ and $\hat{L}_{\text{mean}}$ are calculated . These are then averaged out throughout the measurements upon the z axis displacements, i.e. upon the bar sets of Fig. 11, and are displayed in Fig. 12.

The dependence of the mean estimated inductance $\hat{L}_{\text{mean}}$ upon frequency is displayed on the left of Fig. 12. Error bars depict the measured variations of inductance $\hat{L}_{\text{max}}$ and $\hat{L}_{\text{min}}$, whose difference $\Delta\hat{L} = \hat{L}_{\text{max}} - \hat{L}_{\text{min}}$ is plotted on the right of Fig. 12.

As it can be seen, the higher central resonant frequency f^*_{res}, the larger $\hat{L}_{\text{mean}}$ is. This observation is also valied for ΔL; the latter resulting in a better position measurement resolution, as already represented by Fig. 11. In other words, given an inductance $L(x)_{\text{coil}}$, this should be brought to the highest possible resonant frequency so that it delivers the highest sensibility. Nevertheless, all curves tend to show a saturation, meaning that further increasing f^*_{res} does not automatically translate into a larger $\Delta\hat{L}$.

On the other hand, for a given maximal resonance frequency f^*_{res}, $\Delta\hat{L}$ (and thus resolution) can be improved by choosing the biggest inductance value. This conclusion can also be appreciated upon closer inspection of Fig. 11.

D. Immunity of Sensor System

In this work, immunity (or robustness) is tested by measuring the influence of electromagnetic fields in the airgap — common in electric drives— upon the rotor position estimated by the sensor system.

For this test, the drive shown in Fig. 8 is assembled with six-toroidally wound coils [20]. The rotor is eccentrically blocked, and a 40 kHz switching-frequency PWM for current generation is activated. Motor phases are interconnected so that a two pole-pair bearing magnetic field is generated. The amplitude of the current is increased from 1 A to 9 A with 1 A steps, rotating at a fixed 2 Hz electric frequency.

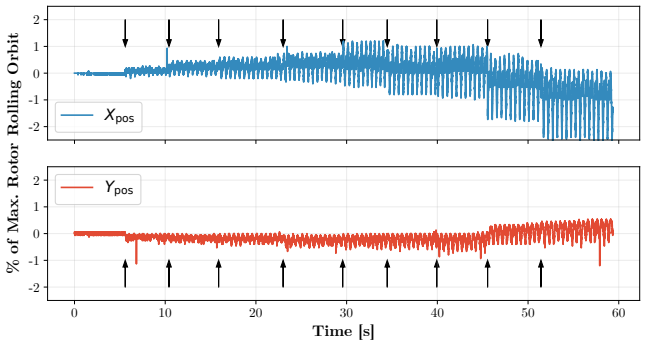

Fig. 13. Influence of two pole-pair field magnetic field of increasing amplitude (marked by arrows) in a slotless motor, generated by PWM-generated currents switched at 40 kHz. The rotor is blocked, and the position offset is removed from the signals. These are shown as a percent of the total amplitude signal of the rotor rolling inside a 1000 μm circular mechanical clearance.

The differential position signals on the x and y axes, using the TDK coils, are recorded at 5 kHz. The position offsets (due to blocked rotor position) are removed, and the position signals are normalized by the amplitude of the circular orbit of the free-rolling rotor upon its mechanical clearance, i.e. 1500 bits. The influence of current and its generated magnetic field upon position signals is displayed in Fig. 13.

The recorded position signals are definitely influenced by the magnetic fields and its associated PWM. Moreover, the larger the current amplitude, the larger the noise. Yet the noise is low in relation to the change in sensor signal due to actual rotor displacement: at the most, 2% deviations can be observed.

A FFT analysis of the power spectrum is done upon the time windows with different excitations, indicated in Fig. 14. The second-harmonic position component increases with excitation, as expected, along a fourth-harmonic component. The latter is probably also generated by the bearing and is picked up by its differential scheme of the sensing coils.

Both Fig. 13 and Fig. 14 display a greater disturbance upon the x axis compared to the y axis. This is because the four sensing coils have a different placement with respect to the six motor coils. The y axis sensing coils lay in front of a motor coil, whereas the x axis sensing coils lay *between* two motor coils; partially between their spacing. The inter-coil installation probably caused the noticeably higher fourth harmonic component; probably due to the different current of the motor coils. This disturbance is almost two order of magnitudes larger in the y axis than in the x axis;

E. Stand-alone position implementation

The two LDC1314s and the Delfino micro-controller are setup so that the latter samples the LDCs at 3.89 kHz. Its differential measurement is then calculated and output upon two of its 12-bit DACs. The outputs are shown in Fig. 16. These outputs can be generally connected to the ADC of another system or micro-controller for magnetic levitation purposes.

V. Conclusion and Outlook

This paper proposes an integrated position system for electrically-conductive targets, in the scope of magnetically levitated drives. A microcontroller and an IC (eventually two ICs, depending on sampling rate requirements) are commissioned and compose the cornerstones of the position estimation system. This system can be assembled together for a relatively low price that can be further optimized.

The microcontroller-IC combination is implemented to excite off-the-market as well as custom PCB micro coils. Due to their micrometer thinness, the later can be easily fit into narrow airgaps, thus not requiring especial constructional constraints in the design of the bearingless motor.

The position-sensor information of a single sensing coil is fundamentally non-linear, but a differential arrangement of the position sensors renders high-resolution, linear position estimation. It was also found that exciting the sensor coils at higher frequencies results in a better position-data resolution.

Additionally, a filtering and shielding scheme are proposed. Its objective is to protect the sensor from undesired electromagnetic effects that may be picked up in the airgap. This approach showed a good immunity, i.e. rather low sensibility against magnetic fields generated by motor coils, whereas practically no PWM noise could be observed. This is a good result, especially considering that the sensing coils were installed adjacent —with practically no mechanical gap— to the motor coils.

Nevertheless, the position estimation system must yet enable the magnetic levitation of a real system. The proposed system

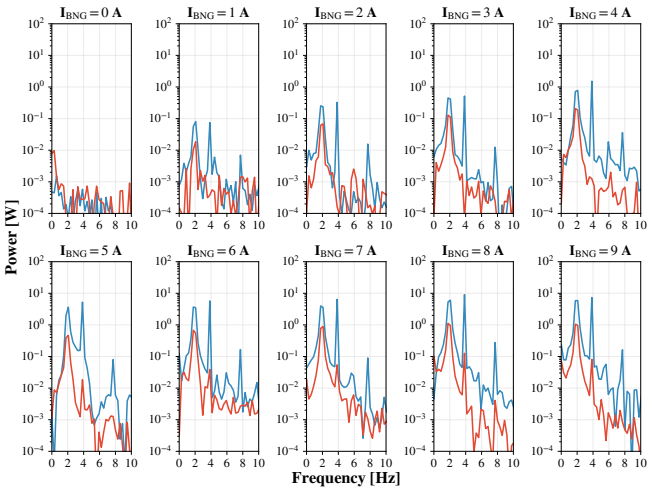

Fig. 14. FFT Power analysis of the fragments of the position signals for different current excitations. The two pole-pair field is detected as a second and fourth harmonic of position displacement. The x axis is more strongly disturbed than the y axis because of its relative position to a coil.

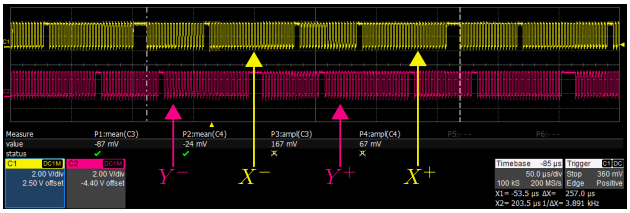

Fig. 15. Double I^2C bus sampling of two LDC1314 circuits. Communication managed by a Launchpad Delfino.

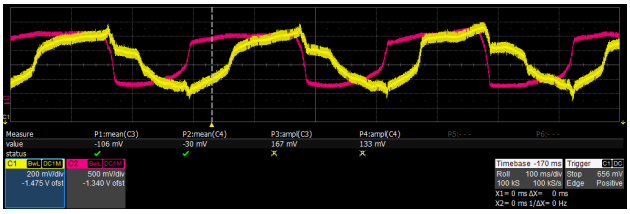

Fig. 16. The x and y differential position measurements at the two outputs of the 12-bit DACs of the Delfino Launchpad. The position of a rotor rolling on a non-perfect airgap with 1000 μm radial clearance is measured.

should be studied in the scope of magnetically-levitated drives that must be axially (instead of radially) stabilized. Further publications might research how various coil shapes affect the target distance range of the sensors.

The accuracy and robustness of the proposed system should also be tested for a slotted motor. The influence of sensing coil placement relative to motor coil placement was perceived in this work, and it should be further studied. Finally, the influence of rotor material, i.e. other rare-earth magnets or ferromagnetic rotor, rotor shape as flux barriers, or rotor bandaging upon sensing resolution and robustness should be investigated.

REFERENCES

[1] A. Chiba, T. Fukao, O. Ichikawa, M. Oshima, M. Takemoto, and D. G. Dorrell, *Magnetic Bearings and Bearingless Drives*. Elsevier, 2005.

[2] J. Zoethout, *Design and integration of position sensing systems*. PhD thesis, Lausanne, 2002.

[3] Schweitzer, Gerhard and E. H. Maslen, *Magnetic Bearings*. 2009.

[4] T. Baumgartner and J. W. Kolar, "Multivariable State Feedback Control of a 500 000-r/min Self-Bearing Permanent-Magnet Motor," *IEEE/ASME Transactions on Mechatronics*, vol. 20, no. 3, pp. 1149–1159, 2015.

[5] A. Sensors, "Eddy Current Sensors," 2019.

[6] L. Precision, "Eddy-Current Displacement & Position Sensors," 2019.

[7] C. M. Zingerli, P. Imoberdorf, J. W. Kolar, and T. Nussbaumer, "Rotor position measurement for a magnetically levitated 500'000 rpm permanent magnet machine," *IEEE ECCE 2011*.

[8] M. Štusák, "Eddy current sensors for magnetic bearings of the textile spinning machines," in *ISMB 2014*, (Linz), pp. 709–713, 2014.

[9] S.-i. Moriyama, K. Watanabe, and T. Haga, "Inductive Sensing System for Active Magnetic Suspension Control," in *ISMB6 1998*, pp. 529–537.

[10] J. Passenbrunner, S. Silber, and W. Amrhein, "Investigation of a digital eddy current sensor," in *2015 IEEE International Electric Machines & Drives Conference (IEMDC)*.

[11] R. P. Jastrzebski, K. Tolsa, and M. Iskanius, "Customization of Digital Circuit for Material Independent Eddy Current Proximity Sensor for Active Magnetic Bearings," in *ISMB 12*.

[12] T. Instruments, "LDC1314 4-channel, 12-bit Inductance-to-Digital Converter with I2C for Inductive Sensing," 2019.

[13] T. Instruments, "LAUNCHXL-F28379D C2000 Delfino MCU F28379D LaunchPad™ development kit — TI.com," 2019.

[14] TDK, "TDK Stacking Proposal for WR111180-36F5-B1 ," 2019.

[15] TI, "Texas Instruments," 2020.

[16] T. Instruments, "EMI Considerationsfor Inductive Sensing," 2020.

[17] R. F. German, H. W. Ott, and C. R. Paul, "Effect of an image plane on printed circuit board radiation," in *IEEE International Symposium on Electromagnetic Compatibility*, pp. 284–291, 1990.

[18] Metglas, "PowerLite C-Cores Technical Bulletin Alloy 2605SA1."

[19] E. Magnetics, "Rare Earth Neodymium NdFeB Magnets Datasheet," 2014.

[20] P. Peralta, D. M. Araujo, and Y. Perriard, "Passive, active and loss tradeoffs in high-speed bearingless motors," in *2018 21st International Conference on Electrical Machines and Systems (ICEMS)*, pp. 162–168, Oct 2018.